Journal of
Applied Crystallography
ISSN 0021-8898

Received 8 March 2011
Accepted 12 August 2011

Comparison of dynamical theory and phase-object approximation for neutron scattering from periodic structures

Rana Ashkar,[a,b]* V. O. de Haan,[c] A. A. van Well,[c] R. Dalgliesh,[d] J. Plomp,[c,d] M. R. Fitzsimmons,[e] W. L. Schaich[b] and Roger Pynn[a,b,f]

[a]Indiana University Center for Exploration of Energy and Matter, Bloomington, IN 47408, USA, [b]Physics Department at Indiana University, Bloomington, IN 47405, USA, [c]Delft University of Technology, Mekelweg 15, 2629 JB Delft, The Netherlands, [d]Rutherford Appleton Laboratory, Chilton, Oxfordshire OX11 0QX, UK, [e]Los Alamos Neutron Science Center, Los Alamos, NM 87545, USA, and [f]Neutron Science Directorate, Oak Ridge National Laboratory, Oak Ridge, TN 37831, USA. Correspondence e-mail: rashkar@indiana.edu

Dynamical theory (DT) calculations have been successfully developed to explain neutron spin-echo resolved grazing-incidence scattering from diffraction gratings. The theory, without any adjustable parameters, has been shown in previous publications to accurately reproduce the sensitivity of the spin-echo polarization signal to sample specifications and scattering geometry. The phase-object approximation (POA), which is computationally less demanding than the DT, has also been used to analyze neutron spin-echo polarization data obtained from diffraction gratings. In this paper, POA and DT calculations are compared for neutron scattering from various diffraction gratings in different geometrical settings. POA gives a good description of the data for transmission cases, where the neutron beam is incident at large angles to the average grating surface. However, for the grazing-incidence reflection cases that were studied, the POA does not fit the data using the independently determined dimensions of the measured gratings. On the other hand, the good agreement between dynamical theory and the data from gratings with known profiles paves the way for its use to extract profile information from periodic samples with unknown structures.

1. Introduction

Since the early use of scattering techniques to study crystal properties, many theories have been developed to explain the scattering data. These theories simulate scattering based on the characteristics of the scattering potential as well as those of the scattered radiation. By fitting a theoretical model to the measured scattering, unknown properties of the sample are extracted. For perfect crystals, a two-beam dynamical theory was proposed by Bethe (1928) to describe dynamical scattering effects of electrons. However, this theory is fairly complicated and when more than two diffracted beams had to be considered the calculations were tedious, especially with the limited computational power available then. Moreover, for most samples (*e.g.* crystals with defects) it is not easy to describe the individual scattering events accurately. Hence, alternative scattering theories involving further approximations were proposed to make calculation schemes easier to evaluate. The challenge has always been to find an approximation that both reasonably models the scattered wave and is readily computed.

In 1957, Cowley & Moodie (1957) proposed a new 'physical-optics' approach to interpret the diffraction of electrons by thin crystals. The authors assumed that, when an electron traverses a region with a varying electrostatic potential, the electron wave at the exit suffers an amplitude modification (due to inelastic scattering) and a phase modification (due to elastic scattering) relative to the incident wave. In the limit where the scattering is perfectly elastic, the effect is due solely to a 'phase-object'. Later, Jap & Glaeser (1978) used a Feynman path formulation to explain the scattering of high-energy electrons from thin specimens with an even simpler approximation, in which the accumulated phase of an electron is calculated along a single classical path parallel to the incident beam direction. This straight-line path approximation is known as the phase-object approximation (POA). A higher-order POA, which involves zigzag as well as straight-line paths, has been also derived (Jap & Glaeser, 1978) and was found, in the case of forward scattering, to be the approximation of Cowley and Moodie.

The POA has been recently applied to small-angle neutron scattering from micrometre-scale silicon diffraction gratings (de Haan *et al.*, 2007). The theoretical approximation allows good fits to the experimental data in the case of transmission but cannot reproduce reflection data without adjustment of some parameters (groove depth and/or period of the grating) (Plomp, 2009; Plomp *et al.*, 2007). This poses a question

regarding the utility of POA for profile retrieval of unknown samples, especially in cases where the scattering is not forward and a straight-line classical approach is not justified.

In systems where the scattering is strong and dynamical effects cannot be neglected, a full dynamical theory approach becomes unavoidable. Exact (to the extent that the scattering is elastic and conserves spin) dynamical theory (DT) calculations have been successfully implemented to describe electron, X-ray and neutron reflection data from diffraction gratings (Berrouane *et al.*, 1992; Neviere *et al.*, 1974; Ott *et al.*, 2001). These DT calculations have usually been limited to a few contributing beams and some authors have reported computational instabilities when higher-order beams were included.

We have recently developed a full dynamical theory calculation, based on a Bloch wave expansion, to interpret spin-echo resolved grazing-incidence scattering measurements from silicon diffraction gratings with nanometre-scale dimensions (Ashkar *et al.*, 2010). The theory is in good agreement with the experimental results and accurately reproduces the sensitivity of the spin-echo polarization signal to slight variations in the sample and beam geometry (Ashkar *et al.*, 2011). The model provides insight into the details of the scattering process and the contribution of different scattered beams to the detected signal. Our calculations show a high degree of stability for all the diffraction orders we have tested (ranging from tens to several hundreds of beams) both in reflection and in transmission geometries.

In this paper, we present comparisons of DT and POA calculations for diffraction gratings in different scattering regimes and for different sample specifications. This is a first step in finding a suitable model for analyzing neutron reflection data from periodic structures. The importance of such modeling techniques lies not in retrieving profile information of periodic surface profiles such as gratings (which can be easily measured by conventional probes such as atomic force microscopy) but in extracting information about buried morphologies that do not extend to the free surface of the sample (*e.g.* viral or polymer assemblies in periodic confinements). If the model is not adequate for describing the scattering phenomenon, fitting it to the data does not necessarily give correct information about the sample. Here, we compare two theoretical models, the DT and the POA, on samples of known structures to test their validity for future use in analyzing periodic samples with more complex morphologies. The notations we use for DT and POA are discussed in §2. The experimental data and the theoretical simulations are presented in §3. We conclude in §4 by a brief discussion on the implications of our results.

2. Theoretical background

In this section, we describe DT and POA calculational schemes for diffraction gratings in two scattering geometries: reflection and transmission. The expressions for DT and POA presented here have been fully developed in previous publications (Ashkar *et al.*, 2010; de Haan *et al.*, 2007; de Haan, 2007). However, the POA notation we use is slightly different from the referenced one. For the sake of clarity, we define the main quantities to be included in the present discussion and we refer the reader for a more detailed description to the publications mentioned above.

The geometry we consider is that of a beam incident on the grating at an angle $(\pi/2 - \theta)$ relative to the z axis, chosen to be perpendicular to the average surface of the grating, and at an angle φ relative to the x axis, chosen along its lines. For completeness, the y axis is perpendicular to the x axis in the plane of the grating. With this choice of reference frame, shown in Fig. 1, the components of the incident neutron wavevector, $\mathbf{k}_0$, are expressed as

$$\begin{aligned} k_{0x} &= k_0 \cos\theta \cos\varphi, \\ k_{0y} &= k_0 \cos\theta \sin\varphi, \\ k_{0z} &= k_0 \sin\theta. \end{aligned} \tag{1}$$

These formulae for the incident wavevector components are common to the DT and POA expressions presented in the following subsections. The components of the scattered neutron wavevector (k_x, k_y and k_z) are measured with respect to the same coordinate system.

2.1. Dynamical theory

In any quantum theory, scattering is studied through the modulation of the incident neutron wave due to its interaction with the scattering potential. In the DT, all multiple scattering effects are taken into consideration and a well defined expression of the neutron wavefunction, $\psi(\mathbf{r})$, is found at any point in the vicinity of the sample. The solution is obtained from the Schrödinger equation:

$$\nabla^2\psi(\mathbf{r}) + [k_0^2 - 4\pi\rho(\mathbf{r})]\psi(\mathbf{r}) = 0. \tag{2}$$

From equation (2), one can see that $\psi(\mathbf{r})$ will depend on the distribution of the scattering length density, $\rho(\mathbf{r})$, within the sample. For a one-dimensional silicon grating with a period d and a groove depth h, $\rho(\mathbf{r})$ is defined as

$$\rho(\mathbf{r}) = \begin{cases} \rho_{\rm air} & \text{if } 0 < z, \\ \rho_{\rm mod}(y, z) & \text{if } -h < z < 0, \\ \rho_{\rm silicon} & \text{if } z < -h. \end{cases} \tag{3}$$

Here, $z = 0$ is at the free surface of the grating and $z = -h$ at the interface between the substrate and the modulated layer, while $\rho_{\rm air}$ ($\rho_{\rm silicon}$) is the neutron scattering length density of air (silicon) and $\rho_{\rm mod}$ is the modulated scattering length density in the region of the grating grooves, which takes values of either $\rho_{\rm air}$ or $\rho_{\rm silicon}$ depending on the shape of the grating lines.

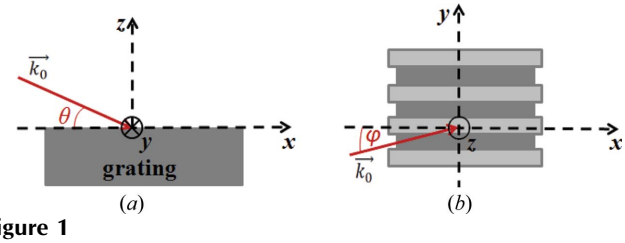

Figure 1
Incident neutron beam geometry in (*a*) the *xz* plane and (*b*) the *xy* plane. The incident beam makes an angle θ with the surface of the grating and an angle φ with its lines.

The translational invariance of the grating along the x axis implies that there is no wavevector transfer along this direction, *i.e.* $k_x = k_{0x}$, whereas the periodicity along the y direction implies that the y component of the wavevector transfer is an integer multiple of the smallest reciprocal lattice vector, $g = 2\pi/d$, of the grating. In other words, $k_y = k_{0y} + mg$. In the case of elastic scattering, the neutron energy must be conserved, which dictates the expressions for the z component of the wavevector of the mth reflected (r) and transmitted (t) wavevector to be

$$k^{\rm r}_{z,m} = [k^2_{0z} + k^2_{0y} - (k_{0y} + mg)^2]^{1/2}, \tag{4a}$$

$$k^{\rm t}_{z,m} = [k^2_{0z} + k^2_{0y} - (k_{0y} + mg)^2 - 4\pi\rho_{\rm silicon}]^{1/2}. \tag{4b}$$

A complete solution requires the determination of the scattering amplitudes of each of the scattered beams. For the present discussion, we will only introduce the expressions for the wavefunction in air and in the substrate:

$$\psi_{\rm air}(\mathbf{r}) = \left[\exp(-ik_{0z}z) + \sum_m R_m \exp(ik^{\rm r}_{z,m}z)\exp(imgy)\right] \times \exp(ik_{0y}y)\exp(ik_{0x}x), \tag{5a}$$

$$\psi_{\rm sub}(\mathbf{r}) = \sum_m T_m \exp(-ik^{\rm t}_{z,m}z)\exp(imgy)\exp(ik_{0y}y)\exp(ik_{0x}x). \tag{5b}$$

The first term in equation (5*a*) represents the incident wave of unit modulus, whereas the second set of terms accounts for the sum of reflected beams, each with an associated reflection amplitude R_m. Equation (5*b*) describes the neutron wavefunction in the substrate as a sum of transmitted beams with transmission amplitudes T_m. All z components of the wavevectors appearing in equations (5*a*) and (5*b*) are either positive real or positive imaginary. The amplitudes R_m and T_m are calculated using the condition of continuity of the wavefunction and its z derivative at the interfaces between the different layers. A full description of the matching problem is presented by Ashkar *et al.* (2010).

The discussion above is general and holds for any grating profile. To solve for R_m and T_m, we expand the neutron wavefunction in the modulated layer in terms of Bloch waves, which we express in terms of the Fourier coefficients of the scattering length density of the grating given by

$$\rho^{\rm mod}_l(z) = \frac{1}{d}\int_{-d/2}^{d/2} {\rm d}y\, \exp(-ilgy)\rho_{\rm mod}(y,z) = \frac{\rho_{\rm silicon}}{l\pi}\sin[\pi l f(z)], \tag{6}$$

where $f(z)$ is the depth-dependent filling factor of the grating and l is an integer. In the case of a rectangular grating, $\rho_{\rm mod}$ does not vary as a function of z within the modulated layer and a three-layer model (air, modulated layer, substrate) is enough to describe the sample. However, when the walls of the grating grooves are not vertical, the filling factor varies with depth and so do the Fourier coefficients, $\rho^{\rm mod}_l$. The problem is solved *via* a Parratt (1954) formalism, in which the modulated layer is divided into thin slices within each of which a vertical wall approximation is used. In this case, the boundary conditions at layer interfaces described above have to be applied at the interfaces between all the thin slices as well as at the interfaces with air and the substrate.

2.2. Phase-object approximation

The POA was originally formulated to study transmission intensities of high-energy particles scattering from relatively thin samples. In this paper, we use the same conventional (forward scattering) straight-line path approach to calculate the intensity of neutrons transmitted through our sample. This is based on the hypothesis that the neutron momentum along the direction of propagation is large enough that the neutron does not significantly deflect as it traverses the scattering field of the sample. To find the transmission amplitude of the beam of diffraction order m, we use equation (9) of de Haan *et al.* (2007) combined with the previous definition of the transmitted wave in our equation (5*b*) so that

$$\exp(-ik_{0x}x)\exp(-ik_{0y}y)\exp(ik_{0z}z)\,\psi_{\rm sub} = \exp[i\Delta\Phi(y)] = \sum_m T_m \exp(imgy), \tag{7}$$

where $\Delta\Phi(y) = \Phi(y) - \Phi_0$ is the difference between the phase $\Phi(y)$ acquired by the neutron as it passes through the modulated layer of the grating and the phase Φ_0 acquired by going through the same thickness of air. From equation (7), we see that the transmission amplitude, T_m, is the mth Fourier coefficient of $\exp[i\Delta\Phi(y)]$. The POA derivation we show here is particular to the sample we used in our transmission measurements, which is a trapezoidal grating with the specifications shown in Fig. 2.

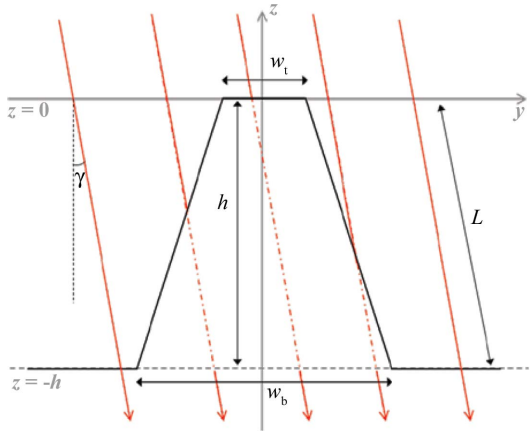

Figure 2
Cross-sectional sketch of one period of the trapezoidal grating with height h and bases of widths $w_{\rm t}$ (top) and $w_{\rm b}$ (bottom). Within the POA, neutrons follow straight-line paths designated by the downward-pointing red arrows. The dashed part of the arrow represents the distance that the neutron covers in silicon before it enters the substrate. The differential phase acquired by a neutron is directly proportional to this distance and varies as a function of y, with the value of y for any path set by where the path crosses into the substrate at $z = -h$.

In the yz scattering plane, the direction of the incident beam is determined by the angle γ defined by $\tan(\gamma) = k_{0y}/k_{0z} = \sin\varphi/\tan\theta$. Also in the yz plane the magnitude of the incident wavevector is $K_0 = (k_{0y}^2 + k_{0z}^2)^{1/2} = k_0\sin(\theta)/\cos(\gamma)$. The phase Φ_0 is defined by $\Phi_0 = K_0 L$, where L is the distance the neutron covers within the modulated layer, given by $L = h/\cos(\gamma)$ as shown in Fig. 2. A similar expression holds for $\Phi(y)$. Consider a beam that goes a distance L_1 in air and a distance L_2 in silicon. The phase acquired along this path is $\Phi(y) = K_0 L_1(y) + K L_2(y)$, where $L_1(y) + L_2(y) = L$ and $K = (K_0^2 - 4\pi\rho_{\rm silicon})^{1/2} \simeq K_0 - 2\pi\rho_{\rm silicon}/K_0$ is the magnitude of the neutron wavevector in silicon. The approximate expression for K is valid in the short-wavelength weak-scattering limit. By substituting for these quantities in the expression for the differential phase we find $\Delta\Phi(y) = -2\pi\rho_{\rm silicon} L_2(y)/K_0$ is directly proportional to the distance L_2 that the neutron covers inside silicon within the modulated layer. If the neutron goes only through silicon, $L_2(y) = L$ and $\Delta\Phi(y) = -2\pi\rho_{\rm silicon} L/K_0 = -\rho_{\rm silicon}\lambda h/\sin(\theta)$, λ being the neutron wavelength.

In general, the differential phase over a period $|y| < d/2$ is given by

$$\Delta\Phi(y) = \frac{-\rho_{\rm silicon}\lambda h}{\sin(\theta)} \times \begin{cases} 0 & \text{if } -d/2 < y < -w_{\rm b}/2 \text{ or } w_{\rm b}/2 < y < d/2, \\ 1 & \text{if } -w_{\rm t}/2 + h\tan(\gamma) < y < w_{\rm t}/2 + h\tan(\gamma), \\ \dfrac{y + w_{\rm b}/2}{(w_{\rm b} - w_{\rm t})/2 + h\tan(\gamma)} & \text{if } -w_{\rm b}/2 < y < -w_{\rm t}/2 + h\tan(\gamma), \\ \dfrac{-y + w_{\rm b}/2}{(w_{\rm b} - w_{\rm t})/2 - h\tan(\gamma)} & \text{if } w_{\rm t}/2 + h\tan(\gamma) < y < w_{\rm b}/2. \end{cases} \tag{8}$$

The equation above holds as long as $\tan(\gamma) < (w_{\rm b} - w_{\rm t})/(2h)$. If this condition is not satisfied then the inclination of the arrows in Fig. 2 is greater than the inclination of the side walls and consequently some of the straight-line paths entering the top of the trapezoid can exit into air before reaching the substrate. In such a case, a different set of equations is needed for $\Delta\Phi(y)$.

The transmission calculations in the POA can be interpreted in a slightly different way. Instead of moving with an angle γ through a symmetrical trapezoid, the scattering geometry can be thought of as normal incidence transmission through a shear-strained trapezoid, with the top base shifted by $h\tan(\gamma)$ along the y axis. The profile of this nonsymmetrical trapezoid is described by the same expression as the piecewise function defined after the curly bracket in equation (8). The prefactor in equation (8) can be thought of as a conventional phase difference expressed as $-\rho_{\rm silicon}\lambda h'$, where h' is the effective height of the grating given by $h' = h/\sin(\theta)$. Of course, the alternative method ends up with the same expression for the differential phase.

Although the early applications of POA were restricted to simulating transmission data from thin specimens, a POA formalism has been recently developed to treat neutron reflectometry from corrugated surfaces (de Haan *et al.*, 2010). Equations for reflectivities in the POA have a different rationale, arising from a modified distorted-wave Born approximation argument (de Haan, 2007). In the present notation they are expressed for a grating with a rectangular profile and a fitting factor f as

$$R_m = \left\{\delta_{0,m} + f[\exp(iq_{z,m}h) - 1]\frac{\sin(m\pi f)}{m\pi f}\right\}\left(\frac{k_{z,m}^{\rm r} - k_{z,m}^{\rm t}}{k_{0z} + k_{z,m}^{\rm t}}\right). \tag{9}$$

In equation (9), $q_{z,m}$ is the z component of the wavevector transfer given by $q_{z,m} = k_{z,m}^{\rm r} + k_{0z}$ and $\sin(m\pi f)/m\pi f = 1$ for $m = 0$. The plus sign in the expression for $q_{z,m}$ is a result of the notation we use for the z component of the incident wavevector [see equation (5*a*)]. The last factor in equation (9) is the so-called 'phase-object enhancement coefficient', which serves to describe the nonforward scattering of a reflection process. In the case of reflection from a flat uniform substrate, m must be zero and the enhancement coefficient becomes the Fresnel reflection amplitude. The factor in curly brackets in equation (9) is the form factor of the grating. We emphasize that this expression for the form factor is valid only for gratings with rectangular profiles, which is the type we used in our reflection measurements. Other expressions for the form factor can be derived for nonrectangular profiles.

2.3. Neutron spin-echo scattering

From this point on, the same analysis holds for the two theoretical approaches. Using the reflection and transmission amplitudes defined above for the DT or POA, we determine the flux of the reflected and transmitted beams from (Pendry, 1974)

$$\Re_m = \frac{k_{z,m}^{\rm r}}{k_{0z}}\left|R_m\right|^2, \quad \Im_m = \frac{k_{z,m}^{\rm t}}{k_{0z}}\left|T_m\right|^2. \tag{10}$$

In calculating $\Re_m$ and $\Im_m$ we exclude beams with imaginary z components of the associated wavevectors because they decay exponentially and hence cannot reach the detector. The exclusion process takes place in the last step of the calculation, which is important to note since, at least in the dynamical theory, these beams do have a significant contribution to the near-field effects, *i.e.* they are important in the boundary-value matching process used to determine the scattering amplitudes.

In a spin-echo scattering angle measurement experiment, one measures the polarization of the outgoing neutron beam, which is the sum of the polarizations of individual scattered beams weighted by their corresponding probabilities. For experiments in which the neutron beam is transmitted through the sample, such experiments are often referred to as SESANS (spin-echo small-angle neutron scattering) measurements, while at grazing incidence, the term spin-echo resolved grazing-incidence scattering (SERGIS) is usually used. In either case, the probability $\tilde{p}_m$ of detecting a diffracted beam of order m is equal to its flux divided by the total measured flux, *i.e.*

$$\tilde{p}_m = \Re_m \Big/ \sum_{m'} \Re_{m'} \quad \text{or} \quad \tilde{p}_m = \Im_m \Big/ \sum_{m'} \Im_{m'}. \tag{11}$$

It is worth mentioning here that, in our transmission cases, the measurements are made at incident angles much larger than the critical angle of the sample material so that the incident beam is totally transmitted. Consequently, the sum of transmitted flux in the denominator of the second equation is unity. This is not true for the grazing-incidence reflection cases, since the incident angle of the neutron beam then may be smaller than the critical angle of silicon for some neutron wavelengths. Furthermore, diffraction events can lead to some $k^{\rm t}_{z,m} > k_{\rm c} = (4\pi\rho_{\rm silicon})^{1/2}$, where $k_{\rm c}$ is the critical wavevector.

The spin-echo polarization of each diffracted beam is given by the cosine of the Larmor phase acquired by that beam during the scattering process, *i.e.* $\cos(q_y y_{\rm se})$. For a beam of order m, $q_y = mg$, as mentioned earlier. The spin-echo length, $y_{\rm se}$, along the coding (y) direction is given by $y_{\rm se} = a\lambda^2$ (Rekveldt, 2003), where a is a constant that depends on the spin-echo setup.

With the above definitions of the probabilities and individual polarizations the total spin-echo polarization signal is then given by

$$P(y_{\rm se})/P_0 = \sum_m \tilde{p}_m \cos(mgy_{\rm se}), \tag{12}$$

where P is the polarization due to scattering from the sample and P_0 is the wavelength-dependent polarization of the setup, obtained from the direct beam (with no sample) for SESANS and from a flat reflecting surface for SERGIS. In either case, P and P_0 should be measured in the same geometry.

3. Data and calculations

The spin-echo experiments described in this paper were carried out at different neutron scattering facilities. Reflection measurements were performed at the OFFSPEC beamline at ISIS and at the ASTERIX beamline at the Los Alamos Neutron Science Center (LANSCE). Transmission data were collected at the Reactor Institute in Delft. Each set of data is a result of 2–4 h of measurement. In this section we compare DT and POA polarization calculations with various sets of reflection and transmission data on diffraction gratings in different scattering geometries.

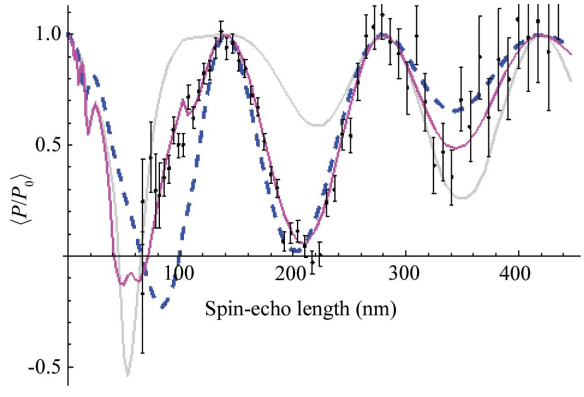

Figure 3
Plot of the spin-echo polarization for reflection from a rectangular grating with d = 140 nm, h = 65 nm and f = 0.5 in the case of grazing incidence ($\theta_0 = 0.2^\circ$) and alignment angle $\varphi_0 = 0.09^\circ$ obtained by 19-beam DT (dark solid line; magenta in the electronic version) and POA (light grey) calculations with $y_{\rm se} = (551{\rm nm}^{-1})\lambda^2$. The dashed line (blue in the electronic version) results from a POA calculation carried out with the same parameters except for h = 34 nm. Data are shown as black points with error bars.

3.1. Reflection

The reflection measurements presented here are SERGIS measurements performed on diffraction gratings. The experiments were motivated by two goals: first, to test the sensitivity of the DT in reproducing experimental results of scattering from gratings with known parameters in different scattering geometries; and second, to test the applicability of the POA and its validity in analyzing reflection data. The ultimate goal is to determine the efficacy of different scattering theories for retrieving profile information from samples with unknown profiles.

The first reflection measurement was carried out at the ASTERIX beamline at LANSCE using the spin-echo setup developed at the Low Energy Neutron Source (LENS) at the Indiana University Center for the Exploration of Energy and Matter (Pynn *et al.*, 2009). The dependence of the spin-echo length on the neutron wavelength is set by the parameters of the setup to be $y_{\rm se} = (551{\rm nm}^{-1})\lambda^2$. With a wavelength range between 0.4 and 0.9 nm, the spin-echo length varies between 88 and 446 nm. The sample we used is a silicon grating with a rectangular profile of period d = 140 nm, groove depth h = 65 nm and filling factor f = 0.5. The specifications of the grating were provided by the manufacturing company (LightSmyth Technologies, Eugene, OR, USA) (measured by scanning electron microscopy) and were confirmed by our own atomic force microscopy measurements. The grating was studied in a grazing-incidence geometry with a nominal incident angle $\theta_0 = 0.2^\circ$.

Dynamical theory calculations for this grating in the scattering geometry of the experiment show very good agreement with the spin-echo data [dark solid line (magenta in the electronic version of the journal) in Fig. 3]. The calculations are based on a 19-beam approximation and a three-layer model determined by the scattering-length-density distribution in the rectangular grating we studied. The parameters used in the theoretical model, such as θ_0, d and h, are all set to their known values. However, the alignment of the grating with the neutron beam was not accurately determined, *i.e.* the nominal alignment angle φ_0 between the incident neutron beam and the lines of the grating was not known to better than 0.1°. With a 0.19° FWHM Gaussian distribution in the angle φ of the incident beam as determined by the configuration of the slits, the best fit to the data is achieved with $\varphi_0 = 0.09^\circ$, which is within the 0.1° experimental uncertainty. The calculation is first performed for fixed values of θ and φ, and then the spin-echo polarization given by equation (12) is averaged over the angular distribution of the incident beam, giving a quantity we denote by $\langle P/P_0 \rangle$. For the measurement described above, we

have a very tight beam collimation in θ so $\langle P/P_0 \rangle$ is an average just over the angular distribution in φ for one value of the incident angle $\theta_0 = 0.2^\circ$.

POA calculations, performed with the same parameters and represented by the solid light-grey line in Fig. 3, do not fit the data. Nonetheless, the POA analytical curve peaks at the right positions, *i.e.* at integer multiples of the grating period. However, when the groove depth of the grating is set to h = 34 nm, keeping all other parameters the same as before, the POA shows much better agreement with the data, as shown by the dashed (blue in the electronic version) curve in Fig. 3. This result conveys a very important message: fitting scattering data with a theoretical model might give incorrect information about the sample if the theory is not adequate for describing the scattering phenomenon.

Other sets of reflection data were collected at the OFFSPEC beamline at ISIS (Dalgliesh *et al.*, 2011). The measurements were performed on different silicon gratings, all with rectangular profiles, purchased from LightSmyth (LightSmyth Technologies, Eugene, OR, USA). In this paper, we present two of these data sets. The first is a grazing-incidence scattering measurement on a grating with a period d = 556 nm, a groove depth h = 110 nm and a filling factor f = 0.5 in the case of a nominal angle of incidence $\theta_0 = 0.15^\circ$ and (perfect) alignment angle $\varphi_0 = 0^\circ$. The second set was collected from a grating with parameters identical to those of the first, except for a deeper groove depth h = 140 nm, for an incident angle $\theta_0 = 0.18^\circ$ and an alignment angle $\varphi_0 = 0^\circ$. The angular divergence of the incident beam is determined from the width and separation of the two slits preceding the sample to be an approximately Gaussian distribution in both θ and φ, centered at θ_0 and φ_0, respectively. The standard deviation is 0.01° for the θ distribution and 0.1° for the φ distribution. This is a typical incident beam profile for reflectometry where the neutron beam is tightly collimated in the specular plane and loosely collimated perpendicular to this plane.

DT calculations for these gratings, shown as the solid curves (magenta) in Figs. 4 and 5, reproduce the scattering data with a high degree of sensitivity. We have shown in a previous publication (Ashkar *et al.*, 2011) that the SERGIS technique is very sensitive to small variations in the grating specifications (mainly the period and the groove depth) and to slight differences in the scattering geometry (*i.e.* the incident θ and φ). The dynamical theory accurately reproduces the SERGIS sensitivity without any adjustment of the input parameters.

On the other hand, POA curves, shown as the dashed lines (blue) in Figs. 4 and 5, do not trace the data correctly. Although for some regions of the spin-echo length good agreement with the data is obtained, the overall output of the POA calculations does not resemble the data. In the above two cases we could not find better POA fits by considering a different groove depth of the grating as we did for the previous case shown in Fig. 3. The calculations carried out with a different groove depth also fit the data only over a certain range of spin-echo length but not outside that range.

3.2. Transmission

Spin-echo transmission measurements were performed at the Reactor Institute in Delft (Plomp, 2009) on a silicon grating that has a period and groove depth of several micrometres and a trapezoidal profile, as depicted in Fig. 2. Measurements on this grating were performed for three different incident-beam settings with θ_0 near 90, 45 or 20°. The results were reported by de Haan *et al.* (2007), along with a POA analysis. More recently, the instrument calibration has been reevaluated, causing some changes to the experimental results and necessitating a new analysis. Unlike the gratings used for the reflection experiments, we do not have independent measurements of the parameters of the trapezoidal grating. Hence, in the fitting process both the grating parameters (d, h, w_t and w_b) and the incident angles (θ_0 and φ_0) are open to adjustment. The revised data and POA fits are shown in Figs. 6–8. The new fit parameters are period d = 11.5 µm,

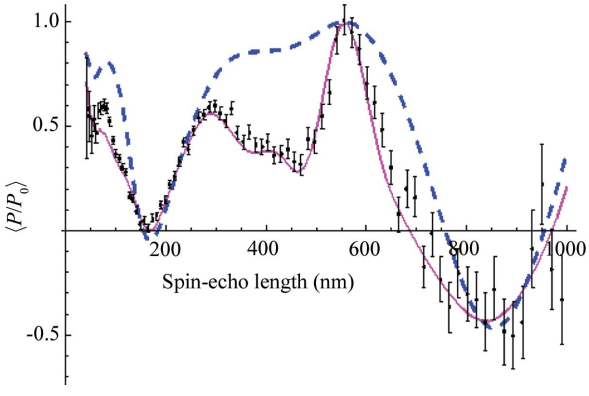

Figure 4
Spin-echo reflection data (points with error bars) on a rectangular grating with d = 556 nm, h = 110 nm and f = 0.5 in the case of grazing incidence ($\theta_0 = 0.15^\circ$) and perfect alignment with the neutron beam ($\varphi_0 = 0^\circ$). The solid line (magenta in the electronic version of the journal) is obtained by a DT calculation and the dashed curve (blue in the electronic version) by a POA calculation. Both calculations use 11 beams and $y_{se} = (10^3\ \mathrm{nm}^{-1})\lambda^2$.

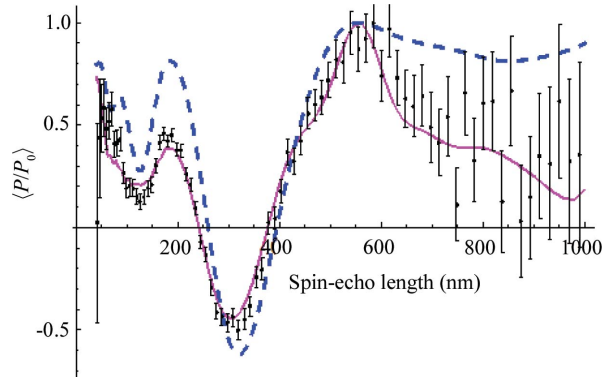

Figure 5
Spin-echo reflection data (points with error bars) from a rectangular grating with d = 556 nm, h = 140 nm and f = 0.5 in the case of grazing incidence ($\theta_0 = 0.18^\circ$) and perfect alignment with the neutron beam ($\varphi_0 = 0^\circ$). Curves are obtained by 11-beam DT (solid, magenta in the electronic version) and POA (dashed, blue) calculations with $y_{se} = (10^3\ \mathrm{nm}^{-1})\lambda^2$.

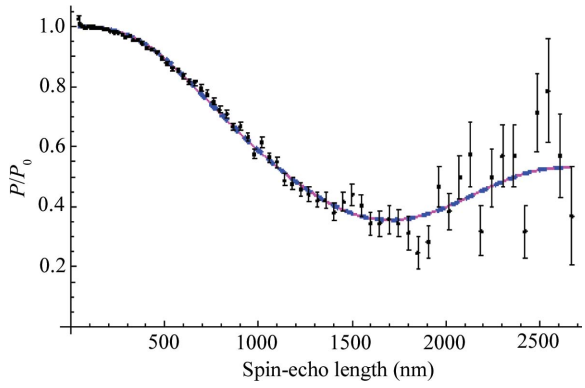

Figure 6
Plot of the spin-echo polarization for neutron transmission from the trapezoidal grating in the case of near normal incidence ($\theta_0 = 88.8^\circ$), with $\varphi_0 = 90^\circ$, obtained by 101-beam DT (solid, magenta) and POA (dashed, blue) calculations with $y_{se} = (4730\text{nm}^{-1})\lambda^2$. The DT model involves 20 slices. Data points are represented by the black dots with error bars.

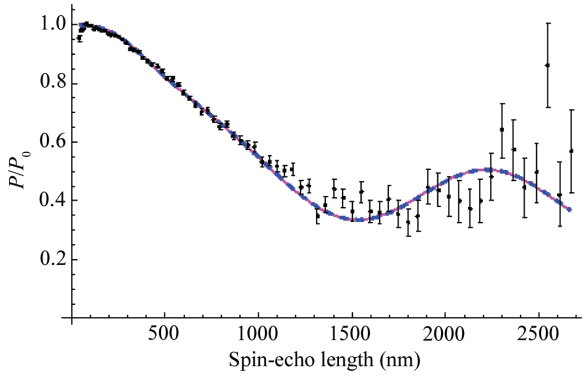

Figure 7
Plot of the spin-echo polarization for neutron transmission from the trapezoidal grating in the case where $\theta_0 = 45^\circ$ and $\theta_0 = 1.6^\circ$ obtained by a 20-slice DT calculation (solid, magenta) and a POA calculation (dashed, blue), both based on a 101-beam approximation with $y_{se} = (4730\,\text{nm}^{-1})\lambda^2$. The black dots with error bars represent the spin-echo data.

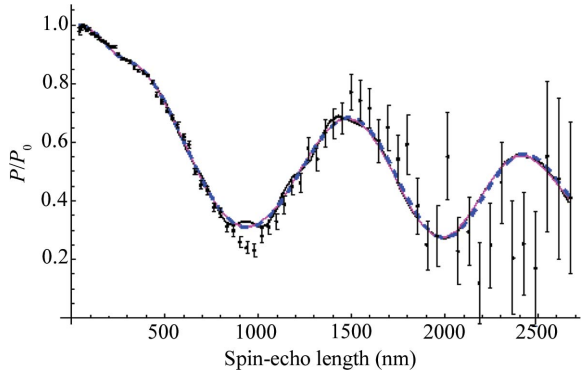

Figure 8
Plot of the transmitted neutron spin-echo polarization for the trapezoidal grating in the case where $\theta_0 = 21.5^\circ$ and $\varphi_0 = 0.75^\circ$. The solid black curve results from a 101-beam DT calculation. The other two curves are obtained by a 20-slice DT calculation (solid, magenta) and a POA calculation (dashed), both including 341 beams with $y_{se} = (4730\text{nm}^{-1})\lambda^2$. The black dots with error bars represent the spin-echo data.

groove depth $h = 46.1$ µm, upper width $w_t = 0.49$ µm and lower width $w_b = 4.41$ µm. For the incident angles (θ_0, φ_0) the three pairs of fitted values are (88.8°, 90°), (45°, 1.6°) and (21.5°, 0.75°). We did not average over distributions in either θ or φ. The results show a reasonable match between experiment and theory, but the large number of fitted parameters leaves open questions of the uncertainty or uniqueness of the fits. Ideally, the experiments should be redone with more accuracy.

However, in this paper, data fitting is not the main concern; instead we want to concentrate on the comparison of POA and DT calculations carried out with the same input parameters. We note that, since the groove sidewalls are not perpendicular to the substrate, DT calculations require the implementation of the Parratt formalism discussed in §2.1. We divide the modulated layer into 20 thin slices of equal thicknesses such that the vertical walls of each thin slice intersect the sidewalls of the trapezoid in the mid-plane of the slice. Figs. 6–8 show that the two calculational schemes give almost identical results in all three cases.

The results require more than a hundred beams in order to produce satisfactory convergence. This larger number of required beams is a result of the period of the grating being more than an order of magnitude greater than the periods of the gratings we used in the reflection experiments. For the first two cases where $(\theta_0, \varphi_0) = (88.8^\circ, 90^\circ)$ and $(45^\circ, 1.6^\circ)$, convergence is obtained for 101 beams, *i.e.* $-50 \leq m \leq 50$. In the last case where $(\theta_0, \varphi_0) = (21.5^\circ, 0.75^\circ)$, 341 beams (*i.e.* $-170 \leq m \leq 170$) are needed to achieve converging results (see Fig. 8). This case is special because the direction of the incident neutron beam is very close to the inclination of the right side wall of the grating in Fig. 2. In the context of POA, this leads to a sharp transition in the acquired phase [see last line in equation (8)], which in turn necessitates the inclusion of more beams (or Fourier components).

4. Conclusions

The comparisons of dynamical theory and phase-object approximation calculations with the neutron scattering data presented in this paper have several implications. First, concerning the DT, the generally good agreement between the calculated spin-echo polarization and the data, both in reflection and in transmission geometries, shows the efficacy of the DT in describing scattering from one-dimensional diffraction gratings. In fact, the DT provides a tractable, computationally exact theory for explaining elastic neutron scattering data from perfectly periodic structures. Moreover, the sensitivity of the theory, as well as the SERGIS technique, to slight variations of sample specifications in reflection measurements indicates the high degree of accuracy with which profile information of the measured sample can be extracted. This theory may now be confidently used to extract profile information about periodic samples with unknown morphologies.

Regarding transmission calculations, although the DT gives a reasonable account of the spin-echo data, alternative theories that are easier and faster to calculate might be a

better option, which leads us to the other set of implications, concerning the POA. That theory matches well our neutron transmission data. It provides a simple and transparent model that explains the scattering data based on the phase modification of the neutron beam within the scattering potential of the sample. The theory, however, is not a suitable model to describe grazing-incidence neutron reflection from our periodic structures. The coincidence that good fits of the POA to the data can be found with parameters that do not resemble the real parameters of the studied sample is a serious concern, making it difficult to know when the theory can be trusted for the extraction of sample dimensions other than the grating period.

We are currently investigating the accuracy of the POA, as well as other approximate theories such as various forms of the distorted-wave Born approximation, over ranges of parameter variations and in different scattering configurations. For these studies the DT simulations will be used as the assumed universally correct results. Comparisons and conclusions will be presented in due course.

This work was funded by the US Department of Energy through its Office of Basic Energy Sciences, Division of Material Science and Engineering (grant No. DE-FG02-09ER46279). We are grateful to the UK Science and Technology Facilities Council ISIS facility, the Los Alamos Neutron Science Center and the Reactor Institute at Delft for the award of beam time. The Los Alamos Neutron Science Center is funded by the US Department of Energy's Office of Basic Energy Sciences under contract DE-AC52-06NA25396 with Los Alamos National Security LLC. The experiments performed at Delft were financially supported by the Nederlandse Organisatie voor Wetenschappelijk Onderzoek.

References

Ashkar, R., Schaich, W. L., De Haan, V. O., van Well, A. A., Dalgliesh, R. M., Plomp, J. & Pynn, R. (2011). *J. Appl. Phys.* In the press.

Ashkar, R., Stonaha, P., Washington, A. L., Shah, V. R., Fitzsimmons, M. R., Maranville, B., Majkrzak, C. F., Lee, W. T., Schaich, W. L. & Pynn, R. (2010). *J. Appl. Cryst.* **43**, 455–465.

Berrouane, H., André, J. M., Barchewitz, R., Moreno, T., Sammar, A., Khan Malek, C., Pardo, B. & Rivoira, R. (1992). *Nucl. Instrum. Methods Phys. Res. Sect. A*, **312**, 521–530.

Bethe, H. A. (1928). *Ann. Phys.* **87**, 55–129.

Cowley, J. M. & Moodie, A. F. (1957). *Acta Cryst.* **10**, 609–619.

Dalgliesh, R. M., Langridge, S., Plomp, J., de Haan, V. O. & van Well, A. A. (2011). *Physica B*, **406**, 2346–2349.

Haan, V. de (2007). *Coherence Approach to Neutron Propagation in Spin Echo Instruments*, 1st ed. Puttershoek: BonPhysics Research and Investigations.

Haan, V.-O. de, Plomp, J., Bouwman, W. G., Trinker, M., Rekveldt, M. T., Duif, C. P., Jericha, E., Rauch, H. & van Well, A. A. (2007). *J. Appl. Cryst.* **40**, 151–157.

Haan, V. O. de, Plomp, J., Rekveldt, M. T., van Well, A. A., Dalgliesh, R. M., Langridge, S., Böttger, A. J. & Hendrikx, R. (2010). *Phys. Rev. B*, **81**, 094112.

Jap, B. K. & Glaeser, R. M. (1978). *Acta Cryst.* A**34**, 94–102.

Neviere, M., Vincent, P. & Petit, R. (1974). *Nouvelle Revue d'Optique*, **5**, 65–77.

Ott, F., Humbert, P., Fermon, C. & Menelle, A. (2001). *Physica B*, **297**, 189–193.

Parratt, L. G. (1954). *Phys. Rev.* **95**, 359–369.

Pendry, J. B. (1974). *Low Energy Electron Diffraction: the Theory and its Application to Determination of Surface Structure.* New York: Academic Press.

Plomp, J. (2009). PhD thesis, Delft University of Technology, The Netherlands.

Plomp, J., de Haan, V. O., Dalgliesh, R. M., Langridge, S. & van Well, A. A. (2007). *Physica B*, **397**, 76–78.

Pynn, R., Fitzsimmons, M. R., Lee, W. T., Stonaha, P., Shah, V. R., Washington, A. L., Kirby, B. J., Majkrzak, C. F. & Maranville, B. B. (2009). *Physica B*, **404**, 2582–2584.

Rekveldt, M. T. (2003). *J. Appl. Cryst.* **36**, 1301–1306.